

Dynamics of cholesteric structures in an electric field

O. S. Tarasov^{1,2}, A. P. Krekhov^{1,2}, and L. Kramer¹

¹*Physikalisches Institut, Universität Bayreuth, D-95440 Bayreuth, Germany*

²*Institute of Molecule and Crystal Physics, Russian Academy of Sciences, 450075 Ufa, Russia*

(Dated: March 25, 2003)

Motivated by Lehmann-like rotation phenomena in cholesteric drops we study the transverse drift of two types of cholesteric fingers, which form rotating spirals in thin layers of cholesteric liquid crystal in an *ac* or *dc* electric field. We show that electrohydrodynamic effects induced by Carr-Helfrich charge separation or flexoelectric charge generation can describe the drift of cholesteric fingers. We argue that the observed Lehmann-like phenomena can be understood on the same basis.

PACS numbers: 61.30.Gd, 61.30.Jf, 47.20.Ky

One of the most interesting manifestations of macroscopic chirality are cholesteric liquid crystals. In cholesterics, as in nematic liquid crystals, there is long-range orientational order of the elongated molecules along a local axis described by the director \mathbf{n} . Whereas in nematics the elastic forces (or torques) tend to establish a uniform orientation of \mathbf{n} , the chiral molecules in cholesterics lead in equilibrium to a helical arrangement with \mathbf{n} perpendicular to the helix axis. Choosing the axis along z , the structure with pitch p_0 is given by $\mathbf{n} = (\cos \varphi(z), \sin \varphi(z), 0)$, $\varphi = q_0 z$, $q_0 = 2\pi/p_0$.

The helical symmetry leads to interesting dynamical effects. Particularly intriguing is the Lehmann rotation of the director structure in a cholesteric droplet heated from below, described in 1900 [1, 2, 3]. It has not been observed again, which is usually attributed to the influence of surface anchoring. However, the electric analog where the temperature gradient is replaced by a *dc* electric field \mathbf{E} (“electromechanical effect”) has been observed [4]. Traditionally, the explanation is based on phenomenological hydrodynamic considerations, which by symmetry allow for an additional dissipative dynamic coupling between the director and electric field (“electromechanical coupling”) [2, 3]. Strictly speaking, here “hydrodynamic” means that spatial modulations must be slow on the scale of the pitch which is not the case in [4]. In fact, in the experiments the director structure inside the droplet was not a homogeneous helix, but included substantial spay-bend distortions and even defects. Another weakness of the approach is that no underlying mechanism has been identified that would, at least in principle, allow to determine the coefficients involved.

We have investigate for the first time a driving mechanism for chirality-related dynamical phenomena, involving well-established electro-hydrodynamic (EHD) effects. Actually, director rotation is not the best choice to study such phenomena, since special precautions are needed to avoid surface anchoring [4]. Another effect is related to the intrinsic length scale defined by helical symmetry. In a confined geometry this can lead to the spontaneous formation of spatial structures (“cholesteric fingers”) lacking certain reflection symmetries, which under nonequi-

librium conditions results in drift of the structures. This is not affected by surface anchoring. We will show that this drift can be explained by EHD effects and, at the end, return to the rotation phenomena.

Cholesterics placed between two plane parallel electrodes (separation d), providing strong homeotropic (perpendicular to the electrodes) anchoring of \mathbf{n} , can experience unwinding of the helix due to the orienting effect of the electric field and of the boundaries. The unwinding transition, which is typically discontinuous, occurs when a combination of the confinement ratio $C = d/p_0$ and the electric field strength (or applied voltage U) reaches a critical value [5]. Thus, there exists a line in the (U, C) plane where the two phases coexist. Near this line one finds the cholesteric fingers (CFs): elongated structures that are localized or arranged periodically. At least four types of CFs were observed [6]. The director configuration of CF of the first type (CF1) is invariant with respect to a π -rotation about the finger axis [7], whereas CF2 has a mirror symmetry with respect to the midplane of the cell [6, 8], see Figs. 1, 3 (top). The difference in structure of CF1 and CF2 manifests itself in the dynamics. In a *dc* field both fingers are observed to drift perpendicular to their axis [9, 10], whereas in an *ac* field only CF2 drifts [9, 10, 11]. Since CFs also grow along their axis one observes the formation of CF spirals. Most measurements of the transverse drift of CFs are based on the analysis of spiral dynamics.

As the motor of the CF1 drift only the electromechanical coupling has been proposed [10]. The magnitude of the drift velocity estimated with the coupling coefficient taken from droplet rotation-type experiments turns out to be at least one order higher than observed [10]. To explain the drift of CF2 in an *ac* field, several models were proposed [8], including electromechanical coupling. However, these models fail to describe the recently observed falloff of the drift velocity V_{\perp} when the frequency $f = \omega/2\pi$ of the applied electric field approaches the inverse charge relaxation time τ_q [12]. In the experiments the conductivity, and thereby τ_q , was varied by using different concentrations of ionic dopant.

The mechanism we propose is based on flow induced ei-

ther by charge separation through anisotropic conductivity, i.e., the Carr-Helfrich effect, (CF2 under *ac* driving) or by flexoelectric charge generation (CF1 under *dc* driving). We use the standard set of nematodynamic equations for the director \mathbf{n} , the velocity \mathbf{v} (Navier-Stokes equation) in the Stokes approximation (neglect of inertial terms), and the electric field \mathbf{E} [2, 3]. As usual the electric properties of the material are described by a dielectric permittivity tensor $\epsilon_{ij} = \epsilon_{\perp}\delta_{ij} + \epsilon_a n_i n_j$, (ϵ_{\perp} , $\epsilon_{\parallel} = \epsilon_{\perp} + \epsilon_a$ are the permittivities perpendicular and parallel to the director, respectively), the analogous conductivity tensor $\sigma_{ij} = \sigma_{\perp}\delta_{ij} + \sigma_a n_i n_j$, and a flexopolarisation $\mathbf{P}^{fl} = e_1 \mathbf{n}(\nabla \cdot \mathbf{n}) + e_3 (\mathbf{n} \cdot \nabla) \mathbf{n}$. We introduce dimensionless variables $t = \tau_d \tilde{t}$, $\mathbf{r} = d \tilde{\mathbf{r}}$, $\mathbf{E} = (U_0/d) \tilde{\mathbf{E}}$, $\mathbf{P}^{fl} = (\epsilon_0 U_0/d) \tilde{\mathbf{P}}^{fl}$, and charge density $\rho_{el} = (\epsilon_0 U_0/d^2) \tilde{\rho}_{el}$. Here $\tau_d = \gamma_1 d^2 / K_{33}$ is the relevant director relaxation time ($\gamma_1 = \text{rotational viscosity}$, $K_{33} = \text{bend elastic constant}$), $U_0 = \sqrt{K_{33}/\epsilon_0}$ characterizes the typical voltage ($U_0 \approx 1\text{V}$ for the materials used).

We choose the z axis perpendicular to the bounding electrodes and allow for a drift of the structure with velocity V_{\perp} in the x direction, transverse to the finger's long axis by replacing $\partial_t \rightarrow \partial_t - V_{\perp} \partial_x$. Then the equations can be written as (tildes are omitted, $\mathbf{V}_{\perp} = V_{\perp} \hat{x}$)

$$[\partial_t + (\mathbf{v} - \mathbf{V}_{\perp}) \cdot \nabla + \gamma_2 \underline{\underline{\delta}}^{\perp} \underline{\underline{A}} - \mathbf{\Omega} \times] \mathbf{n} = -\underline{\underline{\delta}}^{\perp} \mathbf{h}^r, \quad (1)$$

$$p_{,i} - T_{ji,j}^v + h_k^v n_{k,i} = \rho_{el} E_i - V_{\perp} S_{ji,j}, \quad (2)$$

$$\frac{\tau_q}{\tau_d} [\partial_t + (\mathbf{v} - \mathbf{V}_{\perp}) \cdot \nabla] \rho_{el} + \rho_{el} =$$

$$\nabla \cdot [-\epsilon_{\perp} \xi_H (\mathbf{n} \cdot \mathbf{E}) \mathbf{n} + \mathbf{P}^{fl}]. \quad (3)$$

supplemented by the incompressibility condition $\nabla \cdot \mathbf{v} = 0$, the Poisson equation $\rho_{el} = \nabla \cdot [\epsilon_{\perp} \mathbf{E} + \epsilon_a (\mathbf{n} \cdot \mathbf{E}) \mathbf{n} + \mathbf{P}^{fl}]$, which was already used in the charge conservation equation (3), the electrostatic condition $\nabla \times \mathbf{E} = 0$, and the director normalization $\mathbf{n}^2 = 1$. The notation $f_{,i} = \partial f / \partial x_i$ is used throughout. The generation of space charges is characterized by the Helfrich parameter $\xi_H = \sigma_a / \sigma_{\perp} - \epsilon_a / \epsilon_{\perp}$ in Eq. (3).

The director equation (1) couples to the flow field through the local fluid rotation $\mathbf{\Omega} = (\nabla \times \mathbf{v})/2$ and the hydrodynamic strain tensor $A_{ij} = (v_{i,j} + v_{j,i})/2$ with $\gamma_2' = \gamma_2 / \gamma_1$ and the projection tensor $\delta_{ij}^{\perp} = \delta_{ij} - n_i n_j$. Coupling to the elastic and electric torques is through $h_i^r = \delta F / \delta n_i$ with the free energy density $F = \frac{1}{2} k_1 (\nabla \cdot \mathbf{n})^2 + \frac{1}{2} k_2 (2\pi C + \mathbf{n} \cdot (\nabla \times \mathbf{n}))^2 + \frac{1}{2} k_3 (\mathbf{n} \times (\nabla \times \mathbf{n}))^2 - \frac{1}{2} \epsilon_a (\mathbf{n} \cdot \mathbf{E})^2 - \mathbf{P}^{fl} \cdot \mathbf{E}$. Here $k_i = K_{ii} / K_{33}$ with the elastic constants K_{ii} .

In Eq. (2) the Stokes approximation is justified since the processes of interest are controlled by $\tau_d \sim 1$ s and the charge relaxation time $\tau_q = \epsilon_0 \epsilon_{\perp} / \sigma_{\perp} \sim 10^{-3}$ s, which are much larger than the viscous relaxation time $\tau_v = \rho_m d^2 / \gamma_1 \sim 10^{-6}$ s ($\rho_m = \text{mass density}$). The elastic part of the stress tensor (Ericksen tensor) has been eliminated and the pressure redefined: $p = p_0 + F$ [13]. The viscous stress tensor is $T_{ij}^v = \alpha_1' n_i n_j n_k n_m A_{km} +$

$\alpha_2' n_i N_j + \alpha_3' n_j N_i + \alpha_4' A_{ij} + \alpha_5' n_i n_k A_{kj} + \alpha_6' n_j n_k A_{ki}$, where $\alpha_i' = \alpha_i / \gamma_1$ with the Leslie viscosity coefficients α_i . Moreover $\mathbf{N} = (\partial_t + \mathbf{v} \cdot \nabla) \mathbf{n} - \mathbf{\Omega} \times \mathbf{n}$ and $h_k^v = N_k + \gamma_2' n_j A_{jk}$. The bulk force $\rho_{el} \mathbf{E}$ is the Coulomb force and $S_{ij} = \alpha_2' n_i \partial_x n_j + \alpha_3' n_j \partial_x n_i$.

We solve Eqs.(1)-(3) in a perturbative way: $\mathbf{n} = \mathbf{n}_0 + \mathbf{n}_1 + \dots$, $\mathbf{E} = \mathbf{E}_0 + \mathbf{E}_1 + \dots$, $\mathbf{v} = \mathbf{v}_1 + \dots$, $V_{\perp} = V_{\perp 1} + \dots$, $\rho_{el} = \rho_{el 1} + \dots$. At lowest order the electric charge is neglected. Therefore no bulk force arises in Eq.(2) and thus $\mathbf{v}_0 \equiv 0$. \mathbf{n}_0 and \mathbf{E}_0 are obtained from

$$\underline{\underline{\delta}}_0^{\perp} \mathbf{h}_0^r = 0, \quad \nabla \cdot [\epsilon_{\perp} \mathbf{E}_0 + \epsilon_a (\mathbf{n}_0 \cdot \mathbf{E}_0) \mathbf{n}_0] = 0. \quad (4)$$

We write $\mathbf{E}_0 = E_0 (\hat{z} - \nabla \phi_0) \cos(\omega \tau_d t)$ with E_0 the applied electric field and ϕ_0 the induced potential. Previous results show that the director configurations obtained from Eqs.(4) and the stability diagrams are in good agreement with the experiments [5, 6, 12]. We have solved Eqs.(4) in two dimensions (infinite extension of the CF in the y direction) by a relaxation method.

At first order Eq.(3) gives

$$\begin{aligned} \rho_{el 1} = & -\frac{\cos(\omega \tau_d t) + \omega \tau_q \sin(\omega \tau_d t)}{1 + \omega^2 \tau_q^2} E_0 \epsilon_{\perp} \xi_H \\ & \times \nabla \cdot \{[\mathbf{n}_0 \cdot (\hat{z} - \nabla \phi_0)] \mathbf{n}_0\} \\ & + e_{fl} \nabla \cdot \{ \mathbf{n}_0 (\nabla \cdot \mathbf{n}_0) + \frac{e_3}{e_1} (\mathbf{n}_0 \cdot \nabla) \mathbf{n}_0 \}, \quad (5) \end{aligned}$$

where $e_{fl} = e_1 d / (\epsilon_0 U_0)$. The *dc* case is covered by setting $\omega = 0$. Next one solves the Navier-Stokes Eq.(2) (together with the incompressibility condition) at first order. Taking the *curl* eliminates the pressure and leads to an inhomogeneous ODE for \mathbf{v}_1 with the coefficients depending on \mathbf{n}_0 . The form of the inhomogeneities [right-hand side of (2)] give solution of the form

$$\mathbf{v}_1 = \frac{\epsilon_{\perp} \xi_H E_{eff}^2}{1 + \omega^2 \tau_q^2} \mathbf{f}_1 + e_{fl} E_0 \mathbf{f}_2 + V_{\perp 1} \mathbf{f}_3, \quad (6)$$

where $E_{eff} = E_0 / \sqrt{2}$ (E_0) for *ac* (*dc*) driving and the second term appears only in the *dc* case (then also $\omega = 0$). For the *ac* case a time average of Eq.(2) was taken. The functions \mathbf{f}_i depend only on \mathbf{n}_0 and the α_i' (\mathbf{f}_2 depends also on the ratio of the flexocoefficients e_3 / e_1). We have determined the functions \mathbf{f}_i [from the linearized Eq.(2)] by a Galerkin expansion with trigonometric functions (for CF1) and Hermite polynomials (for CF2) as trial functions.

Finally, the director equation (1) at first order gives

$$\begin{aligned} \underline{\underline{\delta}}_0^{\perp} \mathbf{h}_1^r + \underline{\underline{\delta}}_1^{\perp} \mathbf{h}_0^r = & (\mathbf{v}_1 \cdot \nabla - V_{\perp 1} \partial_x) \mathbf{n}_0 \\ & + \gamma_2' \underline{\underline{\delta}}_0^{\perp} \underline{\underline{A}}_1 \mathbf{n}_0 - \mathbf{\Omega}_1 \times \mathbf{n}_0, \quad (7) \end{aligned}$$

where \mathbf{h}_1^r , $\underline{\underline{\delta}}_1^{\perp}$ are linear in \mathbf{n}_1 . The homogeneous problem $\underline{\underline{\delta}}_0^{\perp} \mathbf{h}_1^r + \underline{\underline{\delta}}_1^{\perp} \mathbf{h}_0^r = 0$ is solved by the translation mode

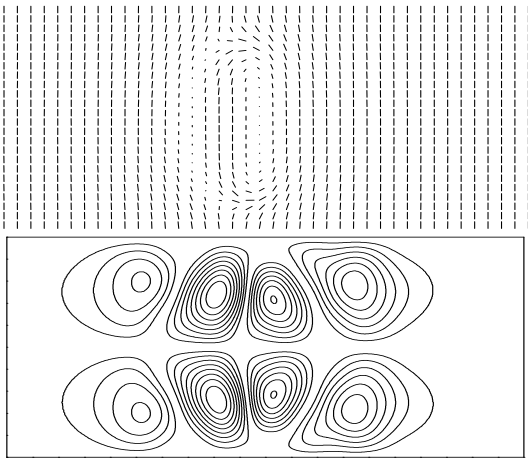


FIG. 1: Director profile (top) and induced velocity profile (stream lines) (bottom) of CF2. $U = 1.9\text{V}$, $\omega\tau_q = 1$, 5CB material parameters [14].

$\partial\mathbf{n}_0/\partial x$. The solvability condition for the inhomogeneous problem [with \mathbf{v}_1 substituted from (6)] fixes the drift velocity $V_{\perp 1}$. In physical units we obtain

$$V_{\perp 1} = \frac{d}{\gamma_1} \frac{\epsilon_0 \epsilon_{\perp} \xi_H}{1 + \omega^2 \tau_q^2} E_{eff}^2 \frac{I_1}{I_0 + I_3} + \frac{e_1 E_0}{\gamma_1} \frac{I_2}{I_0 + I_3}, \quad (8)$$

where $I_0 = \langle \mathbf{n}_{0,x} \cdot \mathbf{n}_{0,x} \rangle$, $I_1 = \langle \mathbf{n}_{0,x} \cdot \mathbf{g}_1 \rangle$, $I_2 = \langle \mathbf{n}_{0,x} \cdot \mathbf{g}_2 \rangle$, $I_3 = \langle \mathbf{n}_{0,x} \cdot \mathbf{g}_3 \rangle$. The last term appears only in the dc case. The functions \mathbf{g}_1 , \mathbf{g}_2 , \mathbf{g}_3 are easily expressed in terms of the \mathbf{f}_1 , \mathbf{f}_2 , \mathbf{f}_3 , respectively. The scalar product is defined by $\langle \mathbf{a} \cdot \mathbf{b} \rangle = \int \int (\mathbf{a} \cdot \mathbf{b}) dx dz$.

We first discuss our results on CF2 drift in an ac field. Since in the experiments the arms of CF2 spirals are well separated [12], we have in the computations chosen a box width large compared to the width of the director structure (isolated finger). The director profile \mathbf{n}_0 together with the stream lines of the flow from (6) as computed for the parameters of the material 5CB (4'-n-pentyl-4-cyanobiphenyl) [14] used in the experiments are shown in Fig. 1. In Fig. 2 our results for $V_{\perp 1}$, which is of order of v_1 , versus reduced frequency $\omega\tau_q$ are shown, together with the experimental results (the different symbols relate to different impurity concentrations between $2 \cdot 10^{-5}$ and 0.05 wt%) [12]. The authors of [12] have scaled the frequency down by a factor of about 1.75 in order to account for the fact that the charge relaxation time τ_q was measured in the isotropic phase at temperature $T = 40 \text{ }^\circ\text{C}$ (the experiments were done at $T = 30 \text{ }^\circ\text{C}$). The three curves correspond to $\sigma_{\parallel}/\sigma_{\perp} = 1.3, 1.4$ and 1.5 , which agrees well with measurements in pure 5CB where $\sigma_{\parallel}/\sigma_{\perp} = 1.44$ [15]. $\sigma_{\parallel}/\sigma_{\perp}$ is the only parameter not given in [12].

Another experimental result born out by the model is the approximate linear dependence of the drift velocity of CF2 as a function of applied field for samples with different thicknesses but fixed confinement ratio C [12].

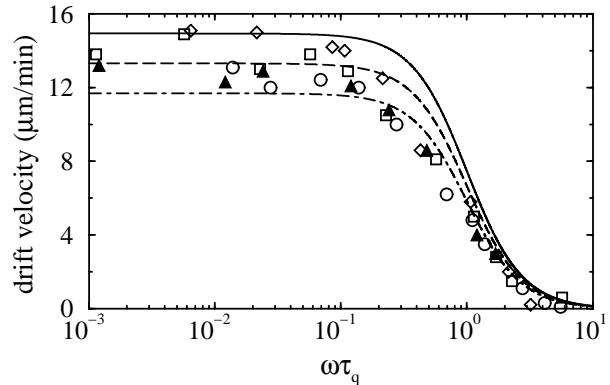


FIG. 2: Drift velocity of CF2 versus reduced frequency: points are experimental data from [12], lines are calculations from (8): for $\sigma_{\parallel}/\sigma_{\perp} = 1.3$ (solid), $\sigma_{\parallel}/\sigma_{\perp} = 1.4$ (dashed), and $\sigma_{\parallel}/\sigma_{\perp} = 1.5$ (dash-dotted). $C = 1.77$, $d = 31 \mu\text{m}$, $U_0 = 1.9 \text{ V}$, 5CB material parameters [14].

The CF2 appear only around an electric field such that $(E_0 d)^2 = \pi^2 / (\epsilon_0 \epsilon_a) (4C^2 K_{22}^2 - K_{33}^2) / K_{33}$ [5]. Using this to eliminate d from (8) one obtains the linear dependence of the drift velocity on E_0 .

We now turn to CF1 in a dc field. From the symmetry of the director profile \mathbf{n}_0 one now has $I_1 = 0$, so one is left with the last term in Eq.(8) relating to flexoelectric charge generation. Unfortunately one now has to cope with various uncertainties. First, the approximation of isolated fingers is not valid, since in the experimental spirals neighboring fingers are packed closely [10, 16]. Second, in the dc case one has to expect screening of the electric field by Debye layers, as evidenced in [16] and also suggested by the voltage offset $\sim 2\text{V}$ in the current-voltage curve presented in [10] [both using the material MBBA (4-methoxy-benzylidene-4'-n-butylaniline)]. Thus we have solved Eqs.(4) on a width

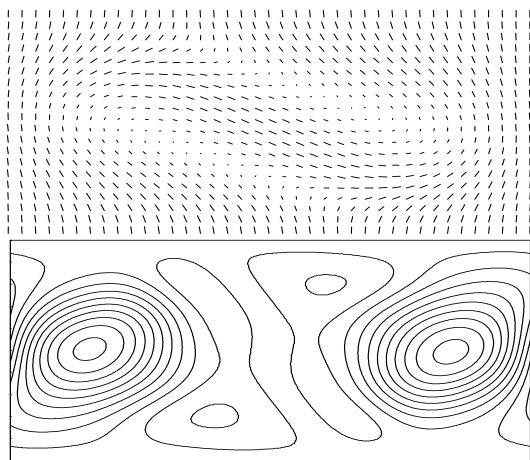


FIG. 3: Director profile (top) and induced velocity profile (stream lines) (bottom) of CF1. $U = 0.2\text{V}$, $L = L_F = 1.95$, MBBA material parameters [17].

L in the x direction with periodic boundary conditions. $V_{\perp 1}$ turns out to be sensitive to L : it decreases with decreasing L and even changes sign at $L \approx 1.6$. In the absence of experimental data on the finger width we have – on one hand – minimized the free energy density with respect to L for given values of the electric field leading to the “optimal” box width $L_F(U)$. Typical values of L_F (in units of d) are $2 \div 2.5$ for a voltage $0.2 \div 3V$. In Fig. 3 an example of the calculated director profile and the stream lines of the flow from (6) are shown. We have

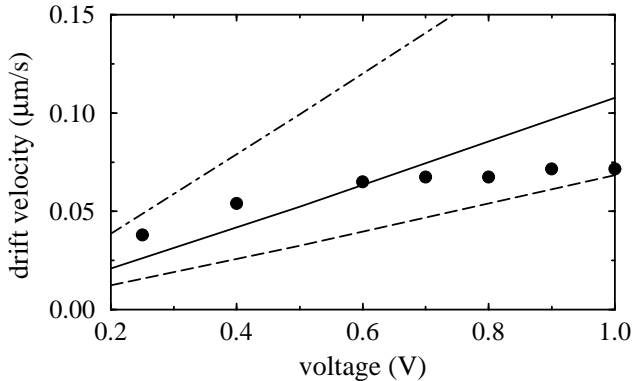


FIG. 4: Drift velocity of CF1 versus voltage: points are experimental data from [10] shifted by 2V; lines are calculations from (8). Solid line: $L = L_F(U)$; dashed: $L = 1.9$; dot-dashed: $L = 2.1$. Flexocoefficients $e_1 = -1.05 \cdot 10^{-11}$ C/m, $e_3 = -1.25 \cdot 10^{-11}$ C/m. $C = 1.14$, $d = 12 \mu\text{m}$, MBBA material parameters [17].

also made calculations for some fixed values of L . Our results for $V_{\perp 1}$ as a function of U , corrected by a screening of 2V, are given in Fig. 4, together with the experimental data [10]. Typical values of the flexocoefficients for pure MBBA were chosen [18].

In conclusion, we have developed an EHD model for the drift of CF1 and CF2. For CF1 in a dc electric field, flow induced by flexoelectric charge generation can describe the drift, but no quantitative conclusion could be drawn. For CF2 a Carr-Helfrich-like mechanism describes *quantitatively* the drift in an ac electric field. Moreover, our preliminary studies show that the EHD model with flexoelectric charge generation (as in CF1) can describe the rotation of cholesteric droplets in a dc electric field [4], which has hitherto been interpreted in terms of phenomenological electromechanical coupling. Furthermore, it seems very likely that analogous thermo-hydrodynamic effects, which lead to very efficient convection phenomena in liquid crystals [19], can also describe the original Lehmann rotation [1]. This then suggests that so far there is no clear experimental manifestation of the (unspecified) phenomenological electro- or thermo-mechanical coupling. The EHD model provides a very

general mechanism for forces and motion that can be applied to other director structures, like other types of cholesteric fingers (CF3 and CF4) and defects in an electric field.

We thank J. Baudry, and P. Oswald for very useful discussions on their experiments and help with the computations of the director structures. Financial support by DFG Grant Kr690/14-1, RFBR Grant 02-02-17435 and the European graduate school “Nonequilibrium phenomena and phase transitions in complex systems” funded by DFG are gratefully acknowledged.

-
- [1] O. Lehmann, *Annalen Phys.* **2**, 649 (1900); C. W. Oseen, *Trans. Faraday Soc.* **29**, 883 (1933).
 - [2] P. G. de Gennes and J. Prost, *The Physics of Liquid Crystals* (Clarendon Press, Oxford, 1993).
 - [3] S. Chandrasekhar, *Liquid Crystals* (Cambridge University Press, 1992).
 - [4] N. V. Madhusudana and R. Pratibha, *Mol. Cryst. Liq. Cryst. Lett.* **5**, 43 (1987); *Liq. Cryst.* **5**, 1827 (1989).
 - [5] P. Oswald, J. Baudry, and S. Pirkl, *Phys. Rep.* **337**, 67 (2000).
 - [6] J. Baudry, S. Pirkl, and P. Oswald, *Phys. Rev. E* **57**, 3038 (1998).
 - [7] M. J. Press and A. S. Arrot, *J. Phys. (France)* **37**, 387 (1976).
 - [8] L. Gil and J. M. Gilli, *Phys. Rev. Lett.* **80**, 5742 (1998).
 - [9] J. M. Gilli and L. Gil, *Liq. Cryst.* **17**, 1 (1994).
 - [10] L. Gil and S. Thiberge, *J. Phys. II (France)* **7**, 1499 (1997).
 - [11] P. Ribiere, P. Oswald, and S. Pirkl, *J. Phys. II (France)* **4**, 127 (1994).
 - [12] J. Baudry, S. Pirkl, and P. Oswald, *Phys. Rev. E* **59**, 5562 (1999); J. Baudry, S. Pirkl, and P. Oswald, *Phys. Rev. E* **60**, 2990 (1999).
 - [13] F. M. Leslie, *Adv. Liq. Cryst.* **4**, 1 (1979).
 - [14] 5CB material parameters used (at 30 °C): viscosities ($\cdot 10^{-3}$ N·s/m²) $\alpha_1 = -6.6$, $\alpha_2 = -77.0$, $\alpha_3 = -4.2$, $\alpha_4 = 63.4$, $\alpha_5 = 62.4$, $\alpha_6 = -18.4$, elastic moduli ($\cdot 10^{-12}$ N) $K_{11} = 3.5$, $K_{22} = 1.6$, $K_{33} = 3.5$ and $\epsilon_{\perp} = 7.3$, $\epsilon_a = 8.9$.
 - [15] J. Jadzyn and P. Kedziora, *Mol. Cryst. Liq. Cryst.* **145**, 17 (1987).
 - [16] H. P. Hinov and E. Kukleva, *Mol. Cryst. Liq. Cryst.* **109**, 203 (1984).
 - [17] MBBA material parameters used (at 25 °C): viscosities ($\cdot 10^{-3}$ N·s/m²) $\alpha_1 = -18.1$, $\alpha_2 = -110.4$, $\alpha_3 = -1.1$, $\alpha_4 = 82.6$, $\alpha_5 = 77.9$, $\alpha_6 = -33.6$, elastic moduli ($\cdot 10^{-12}$ N) $K_{11} = 6.66$, $K_{22} = 4.2$, $K_{33} = 8.61$ and $\epsilon_{\perp} = 5.25$, $\epsilon_a = -0.53$.
 - [18] I. Dozov, Ph. Martinot-Lagarde, and G. Durand, *J. Phys. Lett. (France)* **43**, L-365 (1982); N. V. Madhusudana and G. Durand, *J. Phys. Lett. (France)* **46**, L-195 (1985).
 - [19] see, e.g., L. Kramer and W. Pesch, *Annu. Rev. Fluid Mech.* **27**, 515 (1995).